The 8th European Congress on Computational Methods in Applied Sciences and Engineering
ECCOMAS Congress 2022
5 – 9 June 2022, Oslo, Norway

MATERIAL POINT METHOD FOR LARGE DEFORMATION SEISMIC RESPONSE ANALYSIS

MARC KOHLER[*], ANDREAS STOECKLIN[†] AND ALEXANDER M. PUZRIN[†]

[*] Institute for Geotechnical Engineering
ETH Zurich
Stefano-Franscini-Platz 5, 8093 Zurich, Switzerland
e-mail: marc.kohler@igt.baug.ethz.ch

[†] Institute for Geotechnical Engineering
ETH Zurich
Stefano-Franscini-Platz 5, 8093 Zurich, Switzerland

Key words: Numerical Modelling, Material Point Method, Earthquakes Landslides

Abstract. Landslides triggered by earthquakes are one of the major seismic hazards and can cause large damages and fatalities. The material point method (MPM) has become a popular technique to model such large mass movements. A limitation of existing MPM implementations is the lack of appropriate boundary conditions to perform seismic response analysis of slopes. To bridge this gap, an extension to the basic MPM framework is presented for simulating the seismic triggering and subsequent collapse of slopes within a single analysis step. The concepts of a compliant base boundary and free-field columns are applied within the MPM framework enabling the direct application of input ground motions and accounting for the absorption of outgoing waves.

The presented methodology is applied to an example slope to illustrate the proposed procedure and to benchmark it against the results obtained using an alternative technique, based on a coupled Eulerian Lagrangian (CEL) finite element approach. With the latter approach, the seismic triggering is analysed using a Lagrangian analysis step, followed by an Eulerian step to model the large deformation run-out process. With this procedure, however, the input motion cannot be applied during the runout analysis leading to a potential underestimation of the predicted displacements. This disadvantage can be overcome by the presented “all-in-one” MPM approach. The comparison shows that for short duration ground motions both methodologies lead to almost identical results. For longer earthquake events, on the other hand, the failure mechanism propagates further down- and uphill into stable parts of the slope, when applying the input ground motion throughout the entire analysis, resulting in a considerably larger landslide. Finally, the capability of the presented MPM approach is demonstrated by a simulation of the Tsaoling landslides induced by the 1999 Chi-Chi earthquake in Taiwan.

1 INTRODUCTION

Earthquakes can trigger the failure of slopes and often lead to severe damages and even fatalities. Numerous seismically triggered landslides were reported in the literature that highlight the severity of such catastrophic events [1–4]. Seismic slope stability analysis is therefore a key component for earthquake hazard assessments. Numerous techniques of varying sophistication have been developed in the past, ranging from pseudo-static limiting equilibrium approach, to Newmark's sliding block analysis [5], to stress-deformation analyses [6, 7]. The later has become the state of the art technique and is usually performed using the finite element method (FEM), enabling the use of non-linear constitutive models. To adequately simulate the propagation of seismic waves, appropriate boundary conditions need to be applied to avoid the reflection and trapping of stress-waves within the model domain. Therefore, compliant base boundary conditions [8] and free-field columns [9, 10] have been proposed and successfully implemented for FEM analyses [11].

Once a slope failure is triggered, the velocity of the unstable soil mass increases rapidly and the deformations can become very large. For mesh-based methods (e.g. FEM) special consideration has to be taken due to the problem of excessive mesh distortion. In recent years, a number of advanced techniques have been developed to deal with large deformations [12]. Two of the most frequently used approaches are the coupled Eulerian Lagrangian (CEL) finite element method and the material point method (MPM). However, existing CEL codes do not include appropriate seismic boundary conditions. Therefore, it has been proposed to simulate the seismic triggering using a conventional Lagrangian FEM analysis, followed by a CEL post-failure analysis [13]. The recently proposed implementation of seismic boundary conditions in MPM allows an "all-in-one" approach where the boundary conditions do not have to be changed and the earthquake input motion can be applied during the post-failure as well [14].

In the following, the general concept of MPM is briefly introduced and the framework for seismic analysis including the implementation of appropriate boundary conditions is presented. The framework is described in more detail by Kohler et. al [14]. The procedure is applied to simulate the seismic triggering and subsequent failure of an example slope and the results are compared to a CEL multistep procedure. The capability of the presented MPM approach is demonstrated by a simulation of the Tsaoling landslides induced by the 1999 Chi-Chi earthquake in Taiwan.

2 MPM FRAMEWORK FOR SEISMIC ANALYSIS

2.1 Material point method

The material point method is a hybrid approach, where the material is represented as Lagrangian particles, while the equations of motion are solved on an Eulerian grid [15]. The Lagrangian material representation provides a convenient way of tracking material properties and constitutive variables and to apply Neumann boundary conditions. On the other hand, the Eulerian grid allows the material to undergo large deformations. The general implementation closely follows Stomakhin et al. [16] and Jiang et al. [17], using explicit time integration. The procedure can be described by the 4-step algorithm shown in Figure 1. A crucial part of any

MPM implementation is the transfer back and forth between material points and computational grid. To resolve the often reported problem of grid crossing errors, B-splines are applied for the grid interpolation functions [18, 19]. Dealing with strong nonlinearities, which are often encountered within geotechnical applications and might lead to localizations, cubic B-splines are chosen for this work. In the seismic analysis any Dirichlet boundary conditions are replaced by corresponding external forces and dashpots, which makes the model prone for instabilities at the boundaries and rigid body motions. Therefore, it is important to reach a low kinematic energy in the model prior to the seismic analysis and to choose a stable transfer scheme between material points and grid. The former is guaranteed by the application of local damping where the damping force $\boldsymbol{f}_{d,i}$ is introduced at every grid node proportional to the resulting grid force (or out-of-balance force) $\boldsymbol{f}_i$ and in opposite direction of the grid velocity $\boldsymbol{v}_i$ [20]:

$$\boldsymbol{f}_{d,i} = -sign(\boldsymbol{v}_i)\beta|\boldsymbol{f}_i| \tag{1}$$

where index i refers to grid node i and β is a dimensionless damping factor. The affine particle in cell method (APIC) [17] is a variation of the traditional MPM algorithm and is based on a more stable but only slightly dissipative transfer scheme, which makes it very suitable for the seismic analysis. The key difference to the traditional formulation lies in the mapping of the linear momentum from the material points p to the grid node i, where an additional term to preserve affine velocity fields is considered to conserve the angular momentum [17]:

$$(m\boldsymbol{v})_i = \sum_p m_p w_{ip} \left(\boldsymbol{v}_p + \frac{3}{h^2}\boldsymbol{B}_p(\boldsymbol{x}_i - \boldsymbol{x}_p)\right) \tag{2}$$

where $(m\boldsymbol{v})_i$ is the angular momentum and $\boldsymbol{x}_i$ the position of grid node i, h the grid spacing and w_{ip} the weight of material point p with respect to node i, while the material point quantities are the mass m_p, the velocity $\boldsymbol{v}_p$, the affine matrix $\boldsymbol{B}_p$ and the position $\boldsymbol{x}_p$. The affine matrix at each material point is calculated during the grid to particle step according to:

$$\boldsymbol{B}_p = \sum_i w_{ip}\boldsymbol{v}_i(\boldsymbol{x}_i - \boldsymbol{x}_p)^T \tag{3}$$

where $\boldsymbol{v}_i$ denotes the grid velocity. Because the B-spline basis function range outside of the computation domain and do not maintain unity inside the domain [21], the method of mirrored particles [22] has been applied in this work to enforce kinematic boundary conditions.

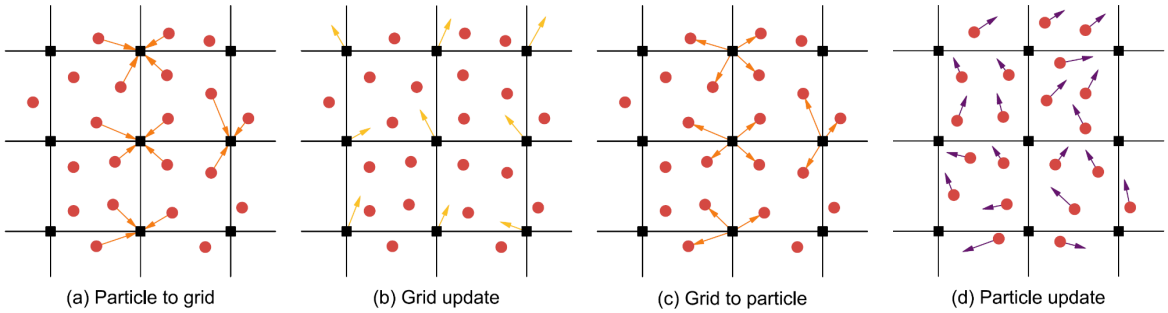

Figure 1: General 4-step algorithm of the MPM: (a) transfer of mass, linear momentum and forces from the material points to the grid, (b) solving the equation of motion on the grid, (c) transfer the updated grid velocities back to the material points and (d) evolve the material points and update the deformation and stress state (after Soga et al., 2016 [12]).

2.2 Seismic modelling procedure

The seismic response of slopes is modelled in two main steps. Firstly, the static stress field within the slope is computed using kinematic boundary conditions. Although the term static is used here, the equation of motion is solved in this step rather than any equilibrium equation. Static conditions are ensured by smoothly ramping up gravity forces over a sufficiently large time period and using local damping according to Equation (1). At the bottom boundary a no-slip condition is used whereas at the lateral boundaries the material points are allowed to move freely in the vertical direction using a slip condition. In a second step, the actual seismic simulation is performed on the same model with different boundary conditions (see Figure 2) which will be described in the following sections. The material points can be carried forward with all the stored information of their constitutive state variables.

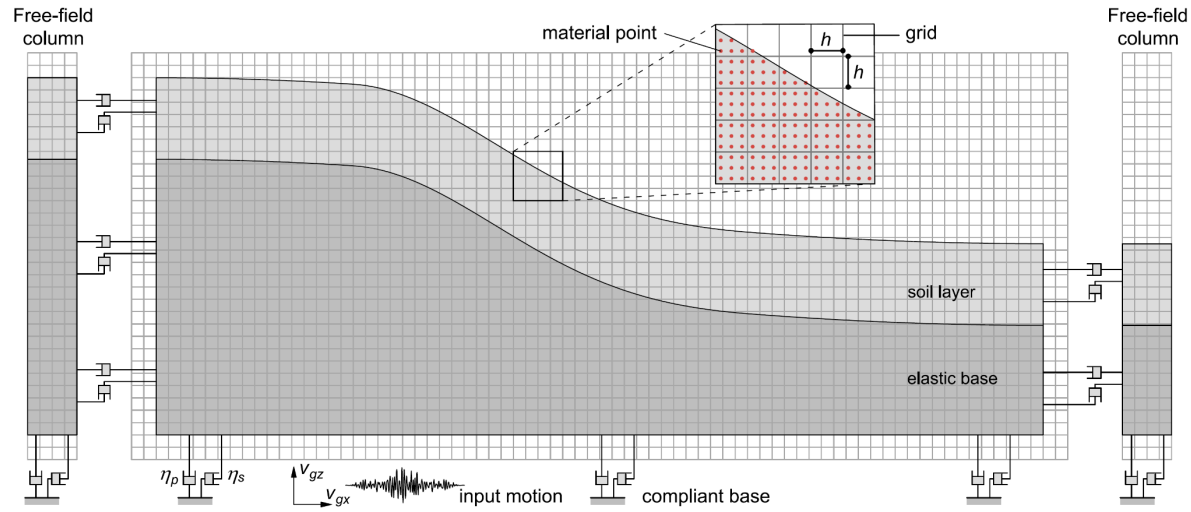

Figure 2: Illustration of the MPM-model for the seismic analysis. The base is modelled as compliant by using wave-absorbing viscous elements. At the lateral boundaries free-field columns are connected to the main model by viscous elements. The earthquake is applied as a traction boundary conditions based on the horizontal and vertical signal of the ground motion.

The base is modelled in the static step by a no-slip boundary using the mirrored particle approach [22]. Therefore, the grid is extended with additional nodes and material points are mirrored across the boundary. These mirrored material points are not explicitly included in the model and only the boundary nodes need a special computational treatment. For the seismic model the mirrored particles are replaced by wave-absorbing viscous elements [8] which are directly applied to the bottom row of material points in the form of a traction force. Similarly, the input motion is applied to the same row of material points as a traction force time history derived from the earthquake signal [23]. Hence, the traction for a bottom material point can be expressed as the sum of three components: (1) a viscous surface traction representing the dashpot element, (2) a reaction force derived from the static analysis and (3) a traction time history representing the applied input ground motion:

$$\boldsymbol{t}_p = \begin{pmatrix} t_{px} \\ t_{py} \end{pmatrix} = \delta_p \begin{pmatrix} \tau_{p,s} + 2v_{su}\sqrt{\rho G} - \eta_s v_{px} \\ \sigma_{p,s} + 2v_{pu}\sqrt{\rho M} - \eta_p v_{py} \end{pmatrix} \tag{4}$$

where δ_p is the surface are related to the material point (see Fig. 3b), v_{px} and v_{py} the material point velocities in the x- and y-direction and $\eta_s = \rho c_s$ and $\eta_p = \rho c_p$ the corresponding dashpot viscosities given by the density ρ and the shear- and pressure-wave speed of the base material. G and M are the shear and P-wave moduli of the base material. The input ground motion is represented by the particle velocity of the upwards propagating shear and pressure wave (v_{su} and v_{pu}). Finally, in order to ensure the static equilibrium of the model by the static shear stress $\tau_{p,s}$ and normal stress $\sigma_{p,s}$ of the corresponding material point are applied as an initial condition and kept constant through the analysis.

Similar to the base boundary, the lateral boundaries are also modelled by the mirrored particle approach for the static analysis. In contrast to the base, a slip boundary is used to allow for vertical deformations. For the seismic analysis the concept of free-field columns is applied [9, 10]. The movement of the free-field columns is not influenced by the main model and hence can either be precomputed or computed in parallel to the main calculation. Free-field conditions are simulated by using periodic boundary conditions in the horizontal direction. The columns are connected to the main model by wave-absorbing dashpot elements. The connection is imposed directly on the boundary material points in the form of a traction force similarly to the bottom boundary. However, the viscous component is defined as a function of the relative motion between the corresponding material points of the free-field (index *fp*) and the main model (index *p*). The traction follows as:

$$\boldsymbol{t}_p = \begin{pmatrix} t_{px} \\ t_{py} \end{pmatrix} = \delta_p \begin{pmatrix} \sigma_{p,s} + \sigma_{fp,d} + \eta_p(v_{fpx} - v_{px}) \\ \tau_{fp,d} + \eta_s(v_{fpy} - v_{py}) \end{pmatrix} \tag{5}$$

where v_{fpx} and v_{fpy} are the velocity components of the material point in the free-field column and v_{px} and v_{py} the corresponding material point velocity in the main model. The viscosities of the dashpots $\eta_s = \rho c_s$ and $\eta_p = \rho c_p$ are given by the shear- and pressure-wave speed of the corresponding material points. Static equilibrium is ensured by the static normal stress component $\sigma_{p,s}$ and is directly applied as traction force f_{ix} to the boundary nodes (Fig. 4) analogously to the base boundary. The seismic stress components $\sigma_{fp,d}$ and $\tau_{fp,d}$ due to the excitation of the free-field columns are given by the dynamic stress tensor of the corresponding fee-field material point as:

$$\boldsymbol{\sigma}_{fp,d} = \boldsymbol{\sigma}_{fp} - \boldsymbol{\sigma}_{fp,s} \tag{6}$$

where $\boldsymbol{\sigma}_{fp}$ is the actual stress tensor and $\boldsymbol{\sigma}_{fp,s}$ the stress tensor at the end of the static analysis of the free-field column. More details on the implementations are presented by Kohler et al. [14].

3 BENCHMARK ANALYSIS

To benchmark the proposed MPM procedure, the example case of a 10m thick soil layer on top of an elastic base with an Gaussian shape [24] is analysed. A linear elastic constitutive model is used in combination with a von Mises model with isotropic softening to model the material behavior of the soil layer. The resulting stress-strain response is linear and elastic up to the peak shear strength, followed by a linear softening until the residual shear strength is reached, from which point onwards it remains constant. The applied parameters are listed in Table 1. The slope was subjected to two input ground motions recorded during the Loma Prieta event in 1989 (RSN 769, H2 direction) and the Imperial Valley event in 1879 (RSN 165, H2 direction), which were retrieved from the PEER strong motion database [25].

As a comparison the same example is simulated using the alternative methodology proposed by Stoecklin et al. [26]. With this approach, the process is analysed in a sequence of three steps: (1) a Lagrangian static step to compute the pre-failure static stress field, (2) a Lagrangian dynamic analysis step to simulate the earthquake event followed by (3) a CEL post-failure analysis step. The key difference to the MPM methodology is that the triggering of the slope failure and the post-failure analysis are simulated in separate steps, since suitable seismic boundary conditions are not available within the applied CEL framework. Once a slope failure is initiated in the seismic step, the analysis is terminated to avoid excessive mesh distortion and the results are transferred to the CEL framework. In this last analysis step the motion is self-driven and the earthquake motion cannot be applied any further.

Table 1: Parameters for example case analysis

Parameter	Elastic base	Soil layer
Element and grid size h	0.25m	0.25m
Numbers of MP's per grid cell n_{MP}	3x3	3x3
Young's modulus E	250 MPa	40 MPa
Poisson's ratio ν	0.25	0.35
Density ρ	2200 kg/m^3	1800 kg/m^3
Peak v. Mises shear strength q_p	-	70 kPa
Residual v. Mises shear strength q_r	-	39 kPa
Residual shear displacement δ_r	-	0.2 m

3.1 Results of the slope failure analysis

The validation of the presented seismic boundary conditions has been shown by Kohler et al. [14] in a fully elastic simulation where both FEM and MPM lead to exactly the same results when comparing the motion at different points in the slope. Figure 5 shows the resulting displacements and distributions of plastic strains for the elasto-plastic simulation. It can be observed that the slope failure is initiated nearly at the same time in both simulations. The developed failure mechanism is almost identical and slight differences only emerge in terms of the development of secondary shear bands. However, the newly formed toe shows a more distinct difference as in MPM the shear band localizes less and a steeper toe is formed. These difference are most likely attributed to the often reported sticky behavior of MPM [27]. However, this does not affect the main results of this analysis as both the time of initiation and the geometry of the final deposit are remarkably similar. For consistency, the ground motion was stopped in the MPM analysis at the same time when the results were transferred to CEL.

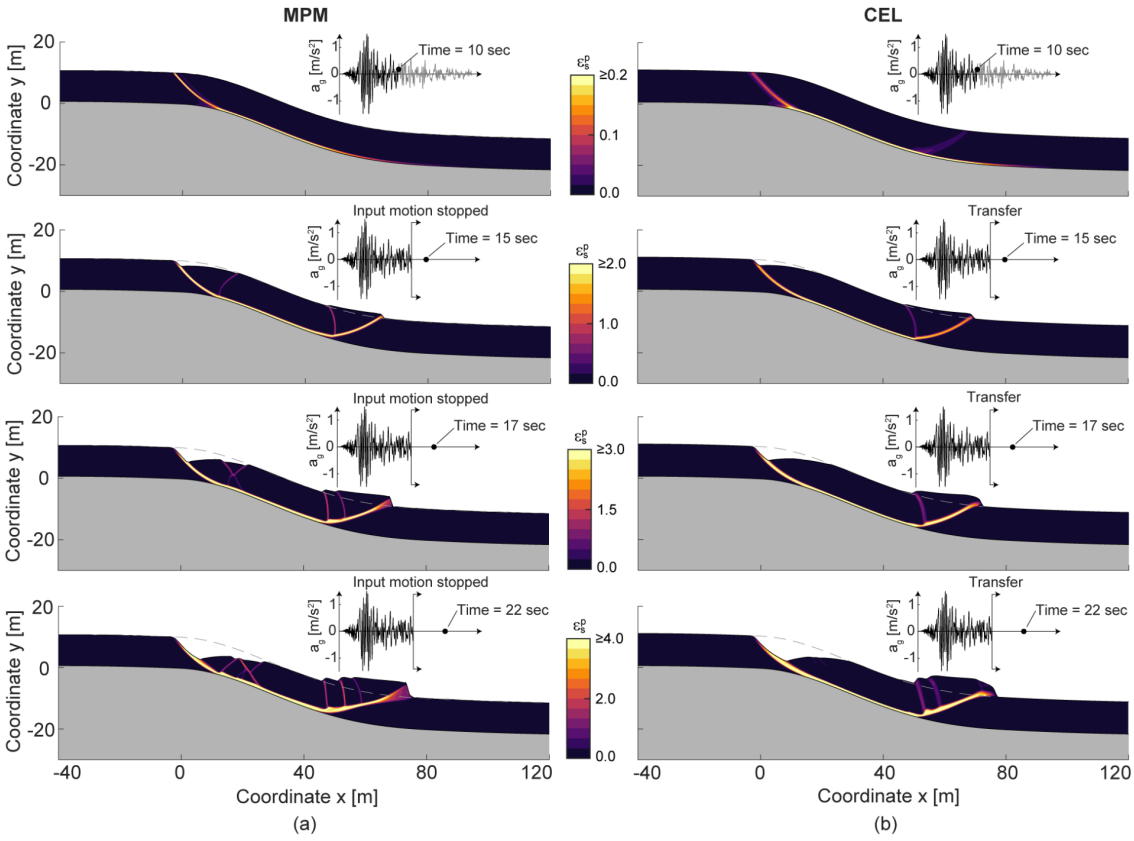

Figure 5: Comparison of the evolution of plastic strain within the example slope at different time points during the analysis for both the MPM (a) and the CEL simulation (b). The slope was subjected to the Loma Prieta (1989) ground motion until the failure became self-driven (after Kohler et al. 2021 [14]).

3.2 Advantages of the MPM procedure

The simplification of stopping the input motion once the slope failure become self-driven is not necessary for MPM. It therefore offers a tool to investigate whether a continuing ground shaking changes the results or not. For the relatively short Loma Prieta ground motion the results are nearly indistinguishable and are not shown here for the sake of brevity. However, as shown in Figure 6, applying the Imperial Valley ground motion, which has a much longer strong motion, leads to significantly different results. The initially triggered failure mechanism is almost identical, but with a continuing ground excitation the failure mechanism propagates further down- and uphill into stable parts of the slope, resulting in a considerably larger landslide. This example analysis demonstrated, that the unified MPM procedure can provide a more reliable risk assessment for certain cases.

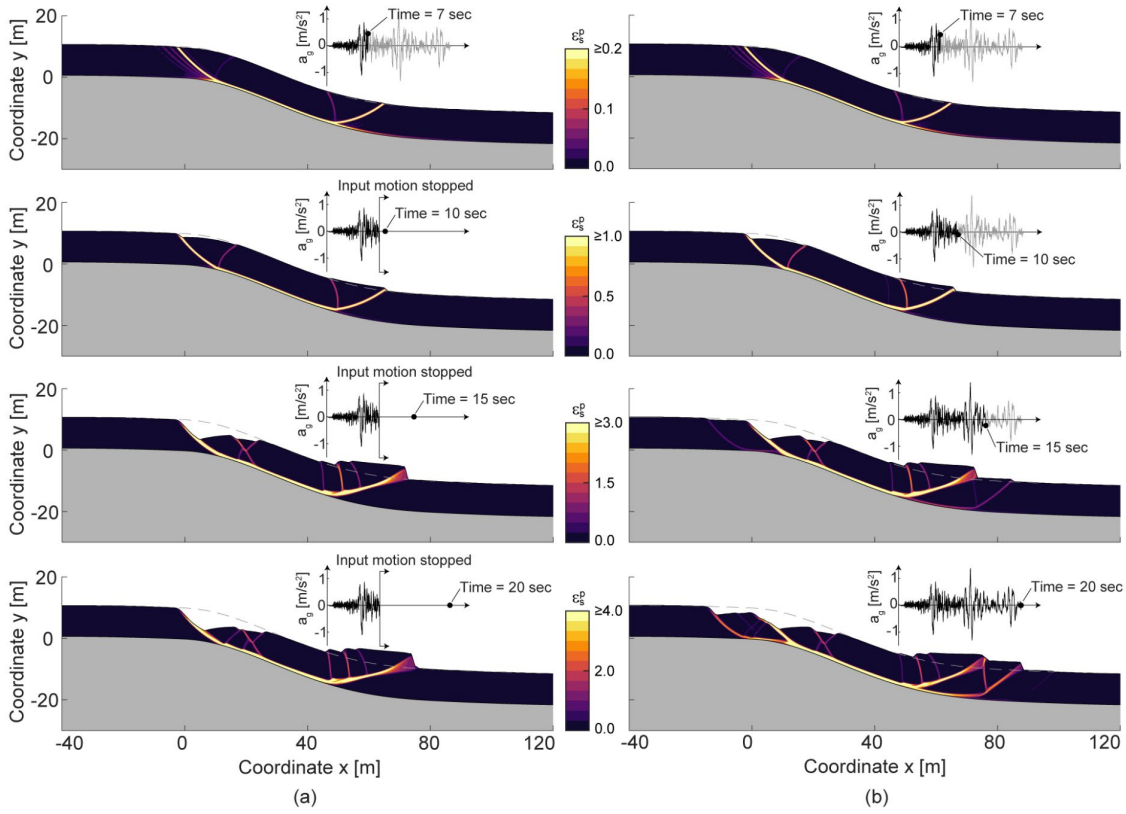

Figure 6: Comparison of the evolution of plastic strains for a model where the motion is applied (a) until the slope becomes self-driven and (b) throughout the entire analysis. The Imperial Valley (RSN 165) recording was applied as an input ground motion (after Kohler et al. 2021 [14]).

4 ANALYSIS OF THE TSAOLING LANDSLIDE

In the following, the presented framework is applied to simulate the catastrophic failure of the Tsaoling landslide. This does not represent an in-depth investigation of this complex event, but rather an illustration and first real case application of the seismic MPM methodology.

4.1 Case and model description

The Tsaoling landslides in Taiwan is the largest slope failure triggered by the 1999 Chi-Chi earthquake, with a volume of about 120Mm^3, and caused 29 fatalities [28]. The rock mass of alternating sandstone and shale beds with a thickness of about 140m failed along distinct bedding planes dipping at an angle of about 14° [29] (Fig. 7a). The shear behaviour of the fault gouge is well investigated due to numerous frictional experiments available in literature [29, 30]. Mizoguchi et al. [31] proposed an exponential slip weakening relation for the friction coefficient of fault gouge as a function of the slip distance d:

$$\mu = \mu_r + (\mu_p - \mu_r)\exp\left(\frac{d \ln 0.05}{d_c}\right) \tag{7}$$

where μ_p and μ_r are the peak and residual friction coefficients and d_c the characteristic slip-distance. This friction model has been implemented in the MPM framework using a Drucker-Prager yield surface matched to a Mohr-Coulomb surface in plane strain for flow at constant volume [32]. The failure plane is introduced in the model as predefined shear zone with thickness δ_s (Fig. 7a), which allows to directly link the slip distance d and the accumulated plastic shear strain ε_s^p assuming simple shear conditions as [14]:

$$\varepsilon_s^p = \frac{d}{\sqrt{3}\delta_s} \tag{8}$$

Because the seismic station CHY080 is located north to the landslide in the Chinshui formation [28], the bedrock is simplified as a uniform linear elastic bedrock neglecting lithological units underneath. The constitutive behavior of the landslide mass (Cholan formation [28]) is modelled using a Mohr-Coulomb yield surface with isotropic softening. The applied parameters are listed in Table 2. The model is subjected to the earthquake motion in vertical and sliding direction. The applied motion was recorded at the CHY080 seismic station [25] located north of the landslide.

Table 2: Parameters for the Tsaoling landslide analyses [28, 29]

Parameter	Bedrock	Landslide mass	Shear zone
Element and grid size h	1.0m	1.0m	1.0m
Numbers of MP's per grid cell n_{MP}	2x2	2x2	2x2
Young's modulus E	3.6 GPa	3.6 GPa	1.0 GPa
Poisson's ratio ν	0.3	0.3	0.3
Density ρ	2580 kg/m^3	2450 kg/m^3	2450 kg/m^3
Peak friction angle φ_p / coefficient μ_i	-	38.5°	0.56
Residual friction angle φ_r / coefficient μ_r	-	18.9°	0.07
Peak cohesion c_p	-	980 kPa	-
Residual cohesion c_r	-	0 kPa	-
Critical slip-distance d_c	-	-	1.7m

4.2 Results

The evolution of velocities and displacements of two selected points are shown in Figure 7b. It can be observed, that the landslides was triggered at the peak impulse, approximately 39s after the rupture of the Chi-Chi earthquake at its epicenter. This finding agrees well with results of 38-40s obtained by Newmark sliding block analysis and survivor's witness [29, 30]. The agreement with the former is not surprising due to the block like sliding at the beginning. However, such Newmark analyses are only capable of modelling the initiation of the landslide. The following computed movement of the landslide mass is characterized by a small number of distinct blocks, which are only fragmented later in the run-out. Inhabitants of a village located on the landslide, reported a similar behaivour [33]. The inhabitants were carried downwards on top of such a block across the Chinshui River and landed on the opposite flank. The computed maximal velocity of 66m/s at Point A is reached after around 70s, which corresponds to the impact of the landslide mass at the bank of the Chinshui River (Fig. 7c). A similar finding was described by Kue et al. [34], who identified high-frequency signals after 76s in the recording at station CHY080 and attributed them to the impact.

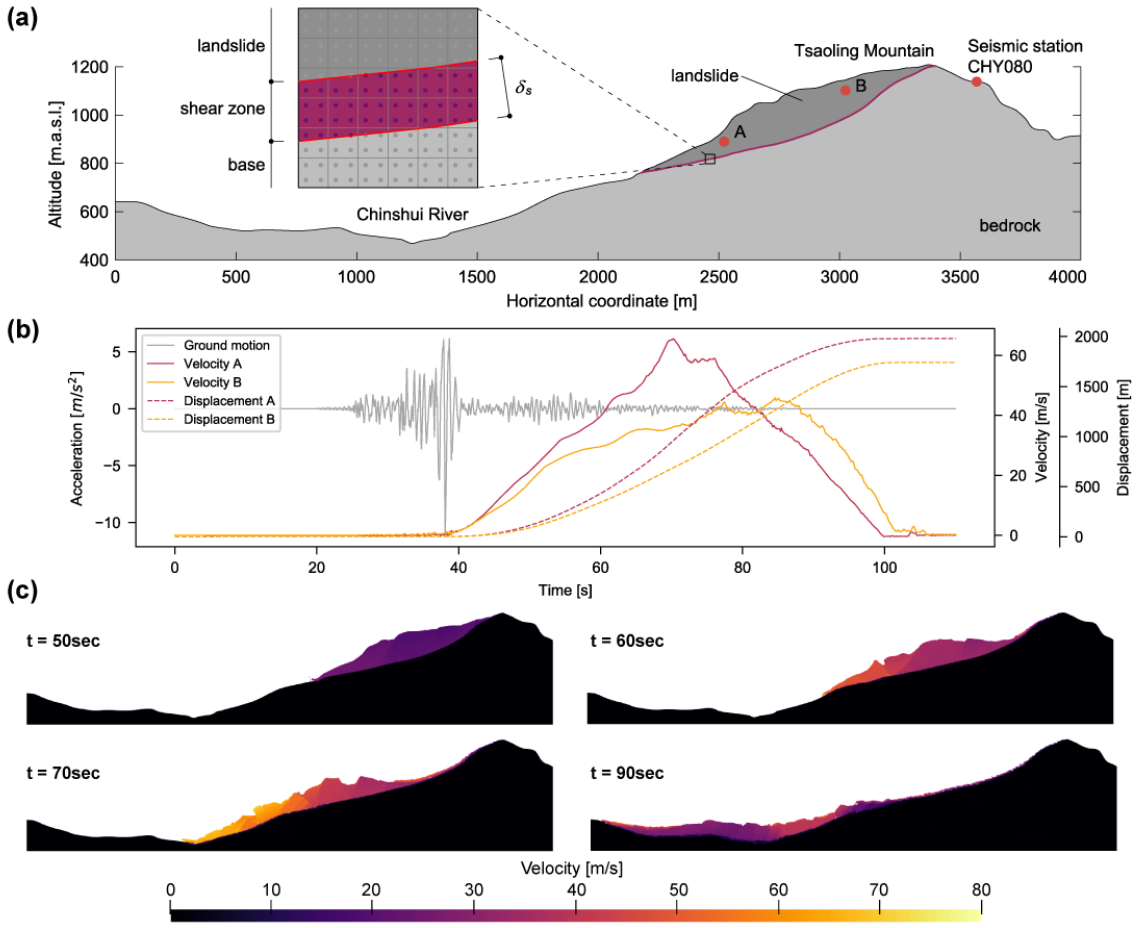

Figure 7: (a) Cross section of the Tsaoling landslide model including the selected output points (after Tang et al. [33]). (b) Evolution of velocities and displacements of two selected points in the landslide. (c) Displacements and velocity distribution at selected times during the landslide failure.

5 CONCLUSIONS

The material point method has become a powerful tool to successfully model large deformation problems in geotechnical engineering. In this work, an extension of the basic MPM framework is presented, for modelling seismic events and successfully benchmarked against an alternative finite element-based approach. The "all-in-one" MPM approach allows for the simulation of seismically triggered landslides within a single analysis step. The presented study highlights that for strong, long duration earthquake events it can be crucial to apply the input motion throughout entire analysis to get a reliable assessment of the expected extent of the triggered landslide event. Finally, the capability of the presented framework is illustrated by simulating the historical catastrophic failure event of the Tsaoling landslide during the 1999 Chi-Chi earthquakes.

REFERENCES

[1] F. C. Dai, C. Xu, X. Yao, L. Xu, X. B. Tu, and Q. M. Gong, "Spatial distribution of landslides triggered by the 2008 Ms 8.0 Wenchuan earthquake, China," *J. Asian Earth Sci.*, vol. 40, no. 4, pp. 883–895, Mar. 2011.

[2] H.-B. Havenith, A. Torgoev, A. Braun, R. Schlögel, and M. Micu, "A new classification of earthquake-induced landslide event sizes based on seismotectonic, topographic, climatic and geologic factors," 2016.

[3] D. K. Keefer, "Investigating landslides caused by earthquakes - A historical review," *Surv. Geophys.*, vol. 23, no. 6, pp. 473–510, 2002.

[4] C. E. Rodríguez, J. J. Bommer, and R. J. Chandler, "Earthquake-induced landslides: 1980-1997," *Soil Dyn. Earthq. Eng.*, vol. 18, no. 5, pp. 325–346, Jul. 1999.

[5] N. M. Newmark, "Effects of Earthquakes on Dams and Embankments," *Géotechnique*, vol. 15, no. 2, pp. 139–160, 1965.

[6] Y. M. a Hashash and D. R. Groholski, "Recent advances in non-linear site response analysis," *Fifth Interantional Conf. Recent Adv. Geotech. Earthq. Eng. Soil Dyn. Symp. Honor Profr. I.M. Idriss*, vol. 29, no. 6, pp. 1–22, 2010.

[7] S. L. Kramer, *Geotechnical Earthquake Engineering*, vol. 6. 1996.

[8] J. Lysmer and R. L. Kuhlemeyer, "Finite Difference Model for Infinite Media," *J. Eng. Mech.*, vol. 95, pp. 859–877, 1969.

[9] J. P. Wolf, "Soil-structure-interaction analysis in time domain," *Nucl. Eng. Des.*, vol. 111, no. 3, pp. 381–393, Feb. 1989.

[10] O. C. Zienkiewicz, N. Bicanic, and F. Q. Shen, "Earthquake Input Definition and the Trasmitting Boundary Conditions," in *Advances in Computational Nonlinear Mechanics*, Vienna: Springer Vienna, 1989, pp. 109–138.

[11] A. H. Nielsen, "Absorbing Boundary Conditions for Seismic Analysis in ABAQUS," *2006 ABAQUS Users' Conf.*, 2006.

[12] K. Soga, E. Alonso, A. Yerro, K. Kumar, and S. Bandara, "Trends in large-deformation analysis of landslide mass movements with particular emphasis on the material point method," *Géotechnique*, vol. 66, no. 3, pp. 248–273, 2016.

[13] A. Stoecklin and A. M. Puzrin, "A combined analysis procedure for submarine landslide evolution," in *Proceedings of the 4th International Symposium on Frontiers in Offshore Geotechnics, ISFOG 2020*, 2020.

[14] M. Kohler, A. Stoecklin, and A. M. Puzrin, "A MPM framework for large deformation seismic response analysis," *Can. Geotech. J.*, Oct. 2021.

[15] D. Sulsky, Z. Chen, and H. L. Schreyer, "A particle method for history-dependent materials," *Comput. Methods Appl. Mech. Eng.*, vol. 118, no. 1–2, pp. 179–196, Sep. 1994.

[16] A. Stomakhin, C. Schroeder, L. Chai, J. Teran, and A. Selle, "A material point method for snow simulation," *ACM Trans. Graph.*, vol. 32, no. 4, p. 1, Jul. 2013.

[17] C. Jiang, A. Selle, J. Teran, and A. Stomakhin, "The Affine Particle-In-Cell Method," *ACM Trans. Graph.*, vol. 34, no. 4, 2015.

[18] M. Steffen, R. M. Kirby, and M. Berzins, "Analysis and reduction of quadrature errors

in the material point method (MPM)," *Int. J. Numer. Methods Eng.*, vol. 76, no. 6, pp. 922–948, Nov. 2008.
[19] R. Tielen, E. Wobbes, M. Möller, and L. Beuth, "A High Order Material Point Method," in *Procedia Engineering*, 2017, vol. 175, pp. 265–272.
[20] P. A. Cundall, "A Discontinuous Future for Numerical Modeling in Soil and Rock," 2002, pp. 3–4.
[21] M. Steffen, P. C. Wallstedt, J. E. Guilkey, R. M. Kirby, and M. Berzins, "Examination and analysis of implementation choices within the Material Point Method (MPM)," *C. - Comput. Model. Eng. Sci.*, vol. 31, no. 2, pp. 107–127, 2008.
[22] S. Schulz and G. Sutmann, "A consistent boundary method for the material point method - using image particles to reduce boundary artefacts," *Int. Conf. Part. Methods*, pp. 522–533, 2019.
[23] L. H. Mejia and E. M. Dawson, "Earthquake deconvolution for FLAC," *Proc. 4th Int. FLAC Symp. Numer. Model. Geomech.*, no. 1969, pp. 1–9, 2006.
[24] E. W. Adams and W. Schlager, "Basic Types of Submarine Slope Curvature," *J. Sediment. Res.*, vol. 70, no. 4, pp. 814–828, Jul. 2000.
[25] T. D. Ancheta *et al.*, "NGA-West2 database," *Earthq. Spectra*, vol. 30, no. 3, pp. 989–1005, Aug. 2014.
[26] A. Stoecklin, P. Trapper, and A. M. Puzrin, "Controlling factors for post-failure evolution of subaqueous landslides," *Géotechnique*, no. 2016, pp. 1–14, 2020.
[27] P. Huang, X. Zhang, S. Ma, and X. Huang, "Contact algorithms for the material point method in impact and penetration simulation," *Int. J. Numer. Methods Eng.*, vol. 85, no. 4, pp. 498–517, Jan. 2011.
[28] T. C. Chen, M. L. Lin, and J. J. Hung, "Pseudostatic analysis of Tsao-Ling rockslide caused by Chi-Chi earthquake," *Eng. Geol.*, vol. 71, no. 1–2, pp. 31–47, Jan. 2004.
[29] T. Togo, T. Shimamoto, J. J. Dong, C. T. Lee, and C. M. Yang, "Triggering and runaway processes of catastrophic Tsaoling landslide induced by the 1999 Taiwan Chi-Chi earthquake, as revealed by high-velocity friction experiments," *Geophys. Res. Lett.*, vol. 41, no. 6, pp. 1907–1915, Mar. 2014.
[30] C. M. Yang *et al.*, "Initiation, movement, and run-out of the giant Tsaoling landslide — What can we learn from a simple rigid block model and a velocity–displacement dependent friction law?," *Eng. Geol.*, vol. 182, no. PB, pp. 158–181, Nov. 2014.
[31] K. Mizoguchi, T. Hirose, T. Shimamoto, and E. Fukuyama, "Reconstruction of seismic faulting by high-velocity friction experiments: An example of the 1995 Kobe earthquake," *Geophys. Res. Lett.*, vol. 34, no. 1, p. 1308, Jan. 2007.
[32] A. M. P. Wedage, N. R. Morgenstern, and D. H. Chan, "A strain rate dependent constitutive model for clays at residual strength," *Can. Geotech. J.*, vol. 35, no. 2, pp. 364–373, 1998.
[33] C. L. Tang *et al.*, "The Tsaoling landslide triggered by the Chi-Chi earthquake, Taiwan: Insights from a discrete element simulation," *Eng. Geol.*, vol. 106, no. 1–2, pp. 1–19, May 2009.
[34] C. Y. Kuo *et al.*, "Simulation of Tsaoling landslide, Taiwan, based on Saint Venant equations over general topography," *Eng. Geol.*, vol. 104, no. 3–4, pp. 181–189, Mar. 2009.